Topology of advective-diffusive scalar transport in laminar flows

M. F. M. Speetjens*
Laboratory for Energy Technology, Eindhoven University of Technology, P. O. Box 513, 5600 MB Eindhoven, Netherlands
(Received 22 June 2007; revised manuscript received 12 October 2007; published 29 February 2008)

The present study proposes a unified Lagrangian transport template for topological description of advective fluid transport and advective-diffusive scalar transport in laminar flows. The key to this unified description is the expression of scalar transport as purely advective transport by the total scalar flux. This admits generalization of the concept of transport topologies known from laminar mixing studies to scalar transport. The study is restricted to two-dimensional systems and the fluid and scalar transport topologies, as a consequence, prove to be Hamiltonian. The unified Lagrangian transport template is demonstrated and investigated for a heat-transfer problem with nonadiabatic boundaries, representing generic scalar transport with permeable boundaries. The fluid and thermal transport topologies under steady conditions both accommodate islands (constituting isolated flow and thermal regions) that undergo Hamiltonian disintegration into chaotic seas upon introducing time periodicity. The thermal transport topology invariably comprises transport conduits that connect the nonadiabatic boundaries and facilitate wall-wall and wall-fluid heat transfer. For steady conditions these transport conduits are regular; for time-periodic conditions these conduits may, depending on degree of diffusion, be regular or chaotic. Regular conduits connect nonadiabatic walls only with specific flow regions; chaotic heat conduits establish connection (and thus heat exchange) of the nonadiabatic walls with the entire flow domain.

DOI: 10.1103/PhysRevE.77.026309 PACS number(s): 47.15.−x, 05.60.−k, 05.45.−a

I. INTRODUCTION

Laminar scalar transport is omnipresent in nature and industry. Consider, for instance, nutrient dispersion in oceanic flows [1,2], magma transport in the Earth's mantle [3], mixing of viscous fluids [4], micromixing [5] or heat and reactant transfer in microreactors [6,7]. Studies to date are predominantly restricted to advective scalar transport, however. The case of advective-diffusive transport, on the other hand, has enjoyed considerably less attention, despite its growing importance due to the miniaturization of equipment (compact heat exchangers, microreactors) and emerging technologies (microfluidics) [6,7]. This is the primary impetus for the present study.

Key quantifiers of advective-diffusive scalar transport are (evolution of) scalar distributions and scalar fluxes. Evolution of scalar distributions is, owing to its great practical relevance, considered predominantly in the context of homogenization. Spectral analyses of the advection-diffusion operator expose the exponential decay of its dominant eigenmodes as a mechanism governing homogenization in steady and unsteady flows alike [8–10]. Such dominant eigenmodes may exhibit intricate spatial structures with fractal properties ("strange eigenmodes") in unsteady flows [11–13]. Intimately related to homogenization are the geometry and dynamics of fronts (e.g., reaction interfaces) [14,15]. Such fronts delineate the flow region where exchange and conversion of material occurs and, consequently, these entities play a fundamental role in the evolution of scalar distributions. Studies specifically on scalar fluxes are mainly restricted to heat-transfer problems involving nonadiabatic boundaries [13,16–18]. The principal objective generally is maximizing heat transfer across the boundaries by increasing the temperature gradients at the fluid-wall interfaces via chaotic advection. Hence, these transport processes rely on heterogenization of scalar distributions.

Lagrangian methods offer insight specifically into the transport mechanisms and transport routes underlying scalar transport. Examples within the scope of homogenization include the Lagrangian filament model [19], describing scalar transport as advective-diffusive transport transverse to filaments formed by fluid advection, stochastic Langevin-type models [20], incorporating diffusion via a stochastic term in the Lagrangian equations of fluid transport, and a Lagrangian diffusion model reducing the original advection-diffusion problem into a diffusion-only problem relative to the fluid-based Lagrangian reference frame [21,22]. In the latter model, the transformation from Eulerian to Lagrangian representation results in an ordinary diffusion equation with a tensor diffusivity; spectral analysis of this tensor, e.g., revealed that for advection-dominated scalar transport the homogenization involves a purely advective initial stage followed by directional diffusive relaxation. A further diffusion-only approach is found in a Lagrangian diffusion model that describes the scalar transport as an effective diffusivity relative to the level sets of the scalar distribution [23]. Both the evolution of scalar distributions (i.e., changes in level sets) and associated scalar fluxes are inextricably linked with this effective diffusivity.

The present study concentrates on identification and analysis of the transport routes demarcated by scalar fluxes and to this end proposes a Lagrangian model that considers scalar transport entirely in terms of advection by the total scalar flux (i.e., by advection and diffusion combined). The rationale underlying this approach is that scalar flux fundamentally is the transport of "scalar parcels" by the total scalar flux in an analogous manner as fluid motion is the transport of fluid parcels by the flow. This advection-only instead

*m.f.m.speetjens@tue.nl

of diffusion-only ansatz sets the proposed Lagrangian model apart from those mentioned before. Principal motivation for the advection-only approach is that it enables generalization of the concept of transport topologies known from Lagrangian mixing studies [4,24,25] to generic advective-diffusive scalar transport and thus paves the way to a unified Lagrangian description for fluid and scalar transport. (Fluid and scalar transport refers to advective and advective-diffusive transport, respectively, hereafter.) The current study is restricted to two-dimensional (2D) bounded systems and the transport topologies of fluid and scalar transport, as a consequence, prove to have a Hamiltonian structure.

The study below is organized as follows. Section II introduces the unified Lagrangian description for fluid and scalar transport. The corresponding Hamiltonian structure—and its implications for the transport topologies—is elaborated in Sec. III. The Lagrangian framework is demonstrated and investigated in Sec. IV for a heat-transfer problem involving nonadiabatic boundaries, representing generic scalar transport problems with scalar flux across boundaries. Conclusions are drawn in Sec. V.

II. UNIFIED LAGRANGIAN TRANSPORT TEMPLATE

Fluid advection and molecular diffusion combined set up a total scalar flux relative to which scalar transport, analogous to fluid transport by the flow field, is purely advective. The Lagrangian representations of the conservation laws for fluid and scalar transport relative to the respective flux fields (i.e., fluid flow and the total scalar flux) are mathematically equivalent. This analogy between fluid and scalar transport forms the basis for the unified Lagrangian transport template proposed below.

The transport of fluid by some given flow field $\boldsymbol{u}$ is in the Lagrangian representation fully described by the position $\boldsymbol{x}(t)$ and corresponding density $\rho[\boldsymbol{x}(t),t]$ of fluid parcels. These properties are governed by

$$\frac{d\boldsymbol{x}}{dt} = \boldsymbol{u}(\boldsymbol{x},t), \quad \frac{\partial \rho}{\partial t} + \boldsymbol{\nabla}\cdot(\rho\boldsymbol{u}) = 0, \tag{1}$$

with initial conditions $\boldsymbol{x}(0)=\boldsymbol{x}_0$ and $\rho(\boldsymbol{x}_0,0)=\rho_0$, where the conservation law corresponds with the continuity equation [26]. The formal solution to the kinematic equation reads $\boldsymbol{x}(t)=\boldsymbol{\Phi}_t(\boldsymbol{x}_0)$ and uniquely determines the current position $\boldsymbol{x}$ for given initial position $\boldsymbol{x}_0$; relation $\boldsymbol{X}(\boldsymbol{x}_0,t)=\boldsymbol{\Phi}_\zeta(\boldsymbol{x}_0)|_{0\le\zeta\le t}$ defines the corresponding trajectory that connects $\boldsymbol{x}_0$ with $\boldsymbol{x}(t)$. Recasting the continuity equation in (1) into the transport form

$$\frac{D}{Dt}(\ln\rho) = -\boldsymbol{\nabla}\cdot\boldsymbol{u}, \tag{2}$$

with $D/Dt=\partial/\partial t+\boldsymbol{u}\cdot\boldsymbol{\nabla}$ the material derivative relative to $\boldsymbol{u}$, reveals that the fluid density ρ is inextricably linked with the rate of divergence of the trajectories $\boldsymbol{X}$. Thus Lagrangian fluid transport is fundamentally determined by the topology of the fluid-parcel trajectories ("flow topology") [27]. The generic make-up of this flow topology, in turn, is fundamentally determined by the continuity equation (Sec. III).

Transport of a scalar ϕ is governed by the conservation law

$$\frac{\partial \phi}{\partial t} + \boldsymbol{\nabla}\cdot(\phi\boldsymbol{u}+\boldsymbol{q}) = 0, \quad \boldsymbol{q} = -\alpha\boldsymbol{\nabla}\phi, \tag{3}$$

with $\phi\boldsymbol{u}$ and $\boldsymbol{q}$ representing advective and diffusive transport, respectively, where α is the diffusivity. Scalar transport admits a Lagrangian representation that is essentially similar to that of fluid transport. Recast to this end relation (3) via the identity $\boldsymbol{\nabla}\phi=\phi\boldsymbol{\nabla}(\ln\phi)$ as

$$\frac{\partial \phi}{\partial t} + \boldsymbol{\nabla}\cdot(\phi\boldsymbol{u}_\phi) = 0, \quad \boldsymbol{u}_\phi = \boldsymbol{u} - \alpha\boldsymbol{\nabla}(\ln\phi), \tag{4}$$

thus resulting in a form akin to the continuity equation in (1), albeit with total scalar flux $\boldsymbol{u}_\phi$ instead of the fluid flow field $\boldsymbol{u}$. [Important to note is that relation (4)—and, inherently, relations deriving from (4)—holds only for $\phi>0$. This condition can readily be fulfilled without loss of generality through proper definition of the scalar ϕ in question [28].] This similarity advances ϕ and $\boldsymbol{u}_\phi$ as analogies to ρ and $\boldsymbol{u}$, respectively. This naturally leads to the concept of "scalar parcels," i.e., virtual parcels with "scalar density" ϕ that are advected by the "scalar flow field" $\boldsymbol{u}_\phi$, as analogy to fluid parcels with density ρ and advected by the flow field $\boldsymbol{u}$. The corresponding Lagrangian representation is, by virtue of the form (4), mathematically identical to (1) and reads as

$$\frac{d\boldsymbol{x}_\phi}{dt} = \boldsymbol{u}_\phi(\boldsymbol{x}_\phi,t), \quad \frac{\partial \phi}{\partial t} + \boldsymbol{\nabla}\cdot(\phi\boldsymbol{u}_\phi) = 0, \tag{5}$$

with appropriate initial conditions. Scalar-parcel trajectories $\boldsymbol{x}_\phi$ are, similar as for fluid parcels, defined by solutions to the kinematic equation in (5). The analogy between (1) and (5) puts forth the notion of a "scalar transport topology," i.e., the topology of scalar-parcel trajectories. This scalar transport topology, due to the mathematical equivalence in underlying conservation laws, has the same fundamental properties as the flow topology.

Both (1) and (4) constitute conservative systems. Relation (1) represents conservation of mass $dm=\rho dV$ of material volumes dV of fluid parcels migrating in the field $\boldsymbol{u}$; relation (4), similarly, represents conservation of "scalar mass" $dm_\phi=\phi dV_\phi$ of "material volumes" dV_ϕ of scalar parcels in the field $\boldsymbol{u}_\phi$. Consider, e.g., thermal transport, in which case ϕ and $\phi\boldsymbol{u}_\phi$ identify with the temperature T and the total heat flux $T\boldsymbol{u}-\alpha\boldsymbol{\nabla}T$, respectively, and $dm_\phi=TdV_\phi$ coincides with the thermal energy of heat-parcel volumes dV_ϕ. The thermal energy dm_ϕ contained in dV_ϕ is conserved and heat exchange between heat-parcel volumes is absent; temperature changes are entirely due to compression and expansion of dV_ϕ during its excursion through the thermal topology. The thermal energy $dE=TdV$ of fluid volumes dV, on the other hand, changes by diffusive heat exchange with neighboring volumes. Important to note is that the conservative nature of systems (1) and (4) concerns mass only; the corresponding fluxes $\boldsymbol{u}$ and $\boldsymbol{u}_\phi$ generally are nonsolenoidal and, inherently, material volumes dV and dV_ϕ are generally not preserved. This fundamental subtlety manifests itself in the particular Hamiltonian structure of the systems (Sec. III).

The analogy between fluid and scalar transport forms the basis for a unified Lagrangian transport template. Introduction of the generic scalar θ and flow field $\boldsymbol{v}$ and nondimensionalization via the rescaling $\boldsymbol{x}'=\boldsymbol{x}/L$, $\boldsymbol{v}'=\boldsymbol{v}/U$, $t'=t/\tau$, and $\theta'=\theta/\Theta$ (L, U, τ, and Θ are typical values for the respective physical quantities), upon dropping primes, yields

$$\frac{d\boldsymbol{x}}{dt}=\mu\boldsymbol{v}(\boldsymbol{x},t), \quad \frac{\partial\theta}{\partial t}+\boldsymbol{\nabla}\cdot(\theta\mu\boldsymbol{v})=0, \quad \boldsymbol{v}=\boldsymbol{u}-\frac{1}{\mathrm{Pe}}\boldsymbol{\nabla}(\ln\theta), \tag{6}$$

as unified nondimensional description for both (1) (fluid transport) and (5) (scalar transport). Variables $\boldsymbol{x}$ and θ represent the position and "density" of a parcel released in the flux field $\boldsymbol{v}$. Said density depends, akin to (2), via $D/Dt(\ln\theta)=-\boldsymbol{\nabla}\cdot\boldsymbol{v}$, with D/Dt the material derivative relative to $\boldsymbol{v}$, entirely upon the transport topology. The corresponding nondimensional parameters are

$$\mu=\frac{U\tau}{L}, \quad \mathrm{Pe}=\frac{UL}{\alpha}, \tag{7}$$

with μ the nondimensional flow strength and Pe the Péclet number that gives the ratio between advective and diffusive transport [29]. This set of parameters is to be complemented by case-specific parameters of the flow field. Relations (6) describe fluid transport for $(\theta,\boldsymbol{v})=(\rho,\boldsymbol{u})$, with Pe vanishing from the system, and scalar transport for $(\theta,\boldsymbol{v})=(\phi,\boldsymbol{u}_\phi)$, with finite Pe [30].

The link between scalar fluxes, described here by the unified Lagrangian approach, and scalar distributions (key quantifiers of scalar transport; see Sec. I) is far from trivial for generic advective-diffusive transport. Consider to this end the intersecting angle γ between the scalar flux $\boldsymbol{v}$ and isolevels of θ (scalar distribution), given by

$$\gamma(\boldsymbol{x},t)=\arcsin\left(\frac{\boldsymbol{v}\cdot\boldsymbol{\nabla}(\ln\theta)}{|\boldsymbol{v}||\boldsymbol{\nabla}(\ln\theta)|}\right), \quad 0\le\gamma\le\frac{\pi}{2}, \tag{8}$$

revealing that γ in general exhibits significant spatio-temporal variation and, consequently, the associated flux-distribution correlation is nontrivial. Trivial cases are basically restricted to purely diffusive transport [$\boldsymbol{v}=-\mathrm{Pe}^{-1}\boldsymbol{\nabla}(\ln\theta)$], with isolevels orthogonal to the scalar flux ($\gamma=\pi/2$), and purely advective transport in steady and solenoidal flow fields [$\boldsymbol{v}=\boldsymbol{u}$; $\boldsymbol{u}\cdot\nabla(\ln\theta)=0$], with isolevels coinciding with the scalar flux ($\gamma=0$).

III. HAMILTONIAN REPRESENTATION OF THE UNIFIED LAGRANGIAN TRANSPORT TEMPLATE

The unified Lagrangian transport template (6) constitutes, by virtue of the associated continuity equation, a conservative system. However, the conserved quantity is the "scalar mass" $dm_\theta=\theta dV_\theta$ instead of the "material volume" dV_θ, meaning the system generally is not volume preserving and has a nonsolenoidal flux $\boldsymbol{v}$ (i.e., $\boldsymbol{\nabla}\cdot\boldsymbol{v}\neq0$). The system nonetheless has a Hamiltonian structure and, consequently, exhibits dynamical behavior that is fundamentally equivalent to that of a conservative system. The particular Hamiltonian structure and its fundamental ramifications for the transport properties are elaborated below for both steady and time-periodic conditions.

Under steady conditions the conservation law in (6) simplifies to $\boldsymbol{\nabla}\cdot(\theta\boldsymbol{v})=0$. This implies a "stream function" ψ, defined by $\theta v_x=\frac{\partial\psi}{\partial y}$ and $\theta v_y=-\frac{\partial\psi}{\partial x}$, and, consequently, the Hamiltonian structure

$$\frac{dx}{dt}=\frac{\mu}{\theta}\frac{\partial\psi}{\partial y}, \quad \frac{dy}{dt}=-\frac{\mu}{\theta}\frac{\partial\psi}{\partial x}, \tag{9}$$

for the parcel transport, with $\psi=\psi(x,y)$ the corresponding Hamiltonian function. The isopleths of ψ delineate the parcel trajectories and thus define the topology. Important to note is that the Hamiltonian ψ—and thereby the steady topology—is independent of the system parameter μ. Parameter μ solely determines the position of a parcel on its trajectory at given time t yet not the trajectory itself.

The kinematic equation (9) results in a Hamiltonian topology, viz. the isopleths of ψ, albeit with a nonsolenoidal flux $\boldsymbol{v}$. This seeming paradox can be explained by the fact that the nonsolenoidality of flux $\boldsymbol{v}$ manifests itself solely in the flow direction and leaves the Hamiltonian structure of the transport topology unaffected. The solenoidal flux $\theta\boldsymbol{v}$, underlying the Hamiltonian ψ, and the nonsolenoidal flux $\boldsymbol{v}$, underlying the parcel dynamics, namely have the same direction and differ only in magnitude, implying identical trajectories yet with different transport rates along these trajectories. This has the fundamental implication that transport topologies of $\theta\boldsymbol{v}$ and $\boldsymbol{v}$ are identical, implying qualitatively equivalent parcel dynamics, and "material volumes" dV_θ undergo net volume-changes only in flow direction. Conservation of "mass" thus restricts the nonsolenoidality of $\boldsymbol{v}$ such that its effect is entirely quantitative and the resultant parcel dynamics are essentially equivalent to that of a conservative system.

The parcel trajectories must, on grounds of continuity of ψ, either be closed or attached to the boundary. This restriction admits two kinds of coherent structures in the steady transport topology: Islands formed by concentric closed trajectories, entrapping and circulating parcels, and channels formed by adjacent trajectories attached to permeable boundary segments, via which parcels cross the boundary [Fig. 1(a)]. Reynolds' transport theorem [31] [applied to the control volume bounded by the dashed line in Fig. 1(a)] implies that such channels cannot suddenly start or terminate in the interior of the flow domain; inlet and outlet must coincide with different permeable boundary segments. Thus channels form "transport conduits" between permeable walls via which wall-wall and wall-fluid exchange of material occurs.

The unsteady transport problem can also be tied to Hamiltonian systems. To this end we recast the conservation law in (6) as

$$\frac{\partial}{\partial x}(\theta\mu v_x)+\frac{\partial}{\partial y}(\theta\mu v_y)+\frac{\partial}{\partial t}(\theta v_t)=0, \tag{10}$$

with $v_t=1$. This enables transformation of the 2D unsteady Lagrangian representation (6) into the analogous three-dimensional (3D) steady representation

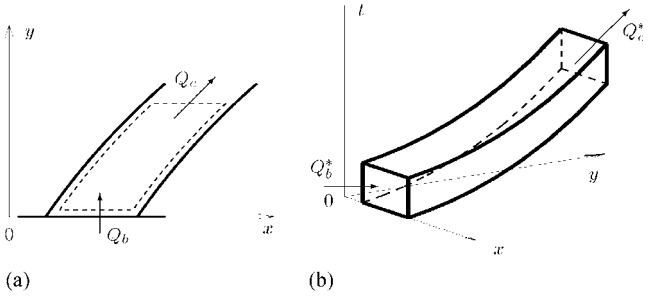

FIG. 1. Formation of channels ("transport conduits") at permeable boundary segments. Panel (a) illustrates the channel formation in the physical domain $\mathcal{D}$ for steady conditions; panel (b) illustrates the channel formation in the time-space domain $\mathcal{D}^*=\mathcal{D}\times[0,t_{\text{end}}]$ for time-periodic conditions. Heavy curves outline channel; $Q_b(Q_b^*)$ indicates inflow via the boundary; $Q_c(Q_c^*)$ indicates through flow in the interior of the channel.

$$\frac{d\boldsymbol{x}^*}{dt}=\boldsymbol{v}^*(\boldsymbol{x}^*),\quad \boldsymbol{\nabla}^*\cdot(\theta\boldsymbol{v}^*)=0, \tag{11}$$

in the time-space domain $\mathcal{D}^*=\mathcal{D}\times[0,t_{\text{end}}]$, with $\boldsymbol{\nabla}^*=(\partial/\partial x,\partial/\partial y,\partial/\partial t)$, $\boldsymbol{x}^*=(x,y,t)$, and $\boldsymbol{v}^*=(\mu v_x,\mu v_y,1)$. The spatio-temporal flow $\theta\boldsymbol{v}^*$ through $\mathcal{D}^*$ is, similar to its counterpart $\theta\boldsymbol{v}$ of the 2D steady case, solenoidal. This implies a vector potential $\boldsymbol{A}$, i.e., $\theta\boldsymbol{v}^*=\boldsymbol{\nabla}^*\times\boldsymbol{A}$, which enables reconciliation of (11) with a 2D unsteady Hamiltonian system [32]. This Hamiltonian representation hinges on vector potentials of the form $\boldsymbol{A}=(A_x,0,A_t)$ that, by definition, are governed by

$$\theta\mu v_x=\frac{\partial A_t}{\partial y},\quad \theta\mu v_y=\frac{\partial A_x}{\partial t}-\frac{\partial A_t}{\partial x},\quad \theta v_t=\theta=-\frac{\partial A_x}{\partial y}. \tag{12}$$

The coordinate transform $\mathcal{F}:\boldsymbol{x}^*\rightarrow\tilde{\boldsymbol{x}}$, with $\tilde{\boldsymbol{x}}=(x,p,t)$ and $p(x,y,t)=-A_x(x,y,t)$, translates system (11) in the physical reference frame $\boldsymbol{x}^*$ into the equivalent system

$$\frac{d\tilde{\boldsymbol{x}}}{dt}=\tilde{\boldsymbol{v}}(\tilde{\boldsymbol{x}}),\quad \tilde{\boldsymbol{v}}=\left(\frac{\partial\psi}{\partial p},-\frac{\partial\psi}{\partial x},v_t\right), \tag{13}$$

with $\psi(x,p,t)=A_t[x,y(x,p,t),t]$, in the canonical reference frame $\tilde{\boldsymbol{x}}$. Here $v_t=1$ and thus the canonical and physical time scales are identical. This leads to

$$\frac{dx}{dt}=\frac{\partial\psi}{\partial p},\quad \frac{dp}{dt}=-\frac{\partial\psi}{\partial x}, \tag{14}$$

as Hamiltonian representation of (6). The latter is in the 2D canonical space (x,p) thus equivalent to a 2D unsteady Hamiltonian system with ψ as corresponding Hamiltonian. Important to note is that, similar as in the steady case, the solenoidal flux $\theta\boldsymbol{v}^*$ and the nonsolenoidal flux $\boldsymbol{v}^*$ have the same direction and differ only in magnitude; the transport topologies of $\theta\boldsymbol{v}^*$ and $\boldsymbol{v}^*$ in the time-space domain $\mathcal{D}^*$ thus are identical, implying, similar as before, qualitatively equivalent spatio-temporal parcel dynamics. Moreover, the above Hamiltonian structure is valid anywhere outside stagnation points of the spatio-temporal flux [32]. Hence, given such stagnation points are nonexistent due to $v_t=1$, the above Hamiltonian structure holds unconditionally for any unsteady system governed by (6).

The time-periodic system may be considered as time-periodic departure from a steady system. This leans on the decomposition $f(\boldsymbol{x},t)=\bar{f}(\boldsymbol{x})+\Delta f(\boldsymbol{x},t)$ of arbitrary time-periodic variables f into its steady and time-periodic components $\bar{f}(\boldsymbol{x})=\int_0^1 f(\boldsymbol{x},\epsilon)d\epsilon$ and $\Delta f(\boldsymbol{x},t)=f(\boldsymbol{x},t)-\bar{f}(\boldsymbol{x})=\Delta f(\boldsymbol{x},t+1)$, respectively. [The nondimensional period time equals unity; τ in (7) corresponds with the physical period time.] Application to (6) yields

$$\frac{\partial}{\partial t}(\dot{\boldsymbol{x}})=\mu\frac{\partial}{\partial t}(\Delta\boldsymbol{v}), \tag{15}$$

as Eulerian time derivative of the parcel trajectories and, inherently, of the topology [33]. Thus time-periodic conditions introduce temporal fluctuations with magnitude $O(\mu)$ in the transport topology. This exposes μ as a measure for the departure from the steady baseline ($\mu=0$).

Diminishing μ means slow parcel motion in the physical domain $\mathcal{D}$, in turn meaning that in the time-space domain $\mathcal{D}^*=\mathcal{D}\times[0,t_{\text{end}}]$ the parcel motion is predominantly in the temporal direction. These conditions, by virtue of the averaging principle known from classical mechanics [34], permit approximation of system (6) by the time-averaged system

$$\frac{d\bar{\boldsymbol{x}}}{dt}=\mu\bar{\boldsymbol{v}}(\boldsymbol{x}),\quad \boldsymbol{\nabla}\cdot(\bar{\theta}\bar{\boldsymbol{v}})=0, \tag{16}$$

in the limit $\mu\rightarrow 0$, with the overbar as before. The time-averaged system (16) is governed by a Hamiltonian $\bar{\psi}$ according to (9) and constitutes the steady baseline upon which the time-periodic system collapses with vanishing μ. The corresponding baseline topology disintegrates with increasing μ following well-known Hamiltonian breakdown scenarios [35]. This results in intricate topologies, typically consisting of regular islands (remnants of the islands of the steady baseline) and chaotic regions, that grow in complexity with increasing μ. An insightful example of such a breakdown may be found in the well-known blinking-vortex flow [35].

The formation of transport conduits between permeable boundary segments is retained under the current time-periodic conditions. Here these conduits form in the time-space domain $\mathcal{D}^*=\mathcal{D}\times[0,t_{\text{end}}]$ in a manner essentially similar as the formation in the physical domain $\mathcal{D}$ under steady conditions. Figure 1(b) shows the formation of such a transport conduit for the time-periodic case on the bottom wall. The conduit consists of the time-space boundary segment $\Gamma_b^*=\Gamma_b\times[0,1]$ (parcel flux across the physical boundary segment Γ_b for one period in time), the time-space cross-section Γ_c^* and the conduit boundary formed by the parcel trajectories $\boldsymbol{X}^*=(X,Y,[0,t])$ in $\mathcal{D}^*$. Inlet and outlet of these transport conduits must, analogous to its steady counterparts, coincide with different permeable boundary segments in the time-space domain. This readily follows from application of Reynolds' transport theorem [31] to (11). This property, in fact,

holds for generic (un)steady systems and thus has the important physical implication that permeable walls imply transport conduits and *vice versa.* The latter form the fundamental topological entities by which scalar exchange between permeable walls and flow occur. The inherently unidirectional flux within the transport conduits, i.e., from one permeable wall (segment) to another, furthermore implies that transport conduits signify essentially heterogeneous transport conditions.

The above exposed the Hamiltonian structure of the unified Lagrangian transport template (6) under both steady and time-periodic conditions and the corresponding universal transport properties. The ramifications for actual fluid and scalar transport are demonstrated and investigated below by way of example.

IV. CASE STUDY: HEAT TRANSFER IN A FLOW BOUNDED BY NONADIABATIC WALLS

A. Introduction

The unified Lagrangian transport template is applied to a heat-transfer problem within the 2D unit square $\mathcal{D}=[0,1]\times[0,1]$. The boundary of $\mathcal{D}$ is impermeable to fluid and has adiabatic sidewalls. Heat exchange with the environment occurs via the "hot" isothermal bottom (temperature $T=2$) wall and "cold" isothermal top wall ($T=1/2$). Thus the thermal boundary conditions read as

$$\left.\frac{\partial T}{\partial x}\right|_{x=0,1}=0, \quad T(x,0,t)=2, \quad T(x,1,t)=\frac{1}{2}, \tag{17}$$

for $0\leq x\leq 1$ and $t\geq 0$. The flow is set up by two counter-rotating point vortices at fixed positions. Considered are a steady ($\boldsymbol{u}_1$) and time-periodic ($\boldsymbol{u}_2$) flow, defined as

$$\boldsymbol{u}_1(\boldsymbol{x})=\frac{1}{2}[\boldsymbol{u}_+(\boldsymbol{x})+\boldsymbol{u}_-(\boldsymbol{x})], \tag{18}$$

$$\boldsymbol{u}_2(\boldsymbol{x},t)=s(t)\boldsymbol{u}_+(\boldsymbol{x})+[1-s(t)]\boldsymbol{u}_-(\boldsymbol{x}), \tag{19}$$

with $\boldsymbol{u}_+$ and $\boldsymbol{u}_-$ the flow fields corresponding with point vortices [36] of constant unit strength situated at $\boldsymbol{x}_+=(1/4,1/2)$ (counterclockwise rotation) and $\boldsymbol{x}_-=(3/4,1/2)$ (clockwise rotation), respectively, and $s(t)=\frac{1}{2}[1+\sin(2\pi t)]$ the time-periodic variation. (Explicit expressions for $\boldsymbol{u}_{+,-}$ are given in the Appendix.) The point-vortex flows have vanishing normal velocity and nonzero tangential velocity on the boundary of the domain $\mathcal{D}$. The domain thus is bounded by solid walls impermeable to fluid. The point-vortex flows introduce no further parameters. Hence μ (time-periodic case only) and Pe according to (7) are the system parameters.

A problem of interest is the heat transfer from the hot bottom wall to the cold top wall through the flow domain as a function of the flow conditions. This involves fluid transport [$\theta=\rho$ and $\boldsymbol{v}=\boldsymbol{u}$ in (6)] and thermal transport [$\theta=T$ and finite Pe in (6)] along fluid-parcel and heat-parcel trajectories, respectively. Flow and thermal topologies are governed by the Hamiltonian function ψ and Ψ, respectively (Sec. III) according to (9) (steady case) and (14) (time-periodic case).

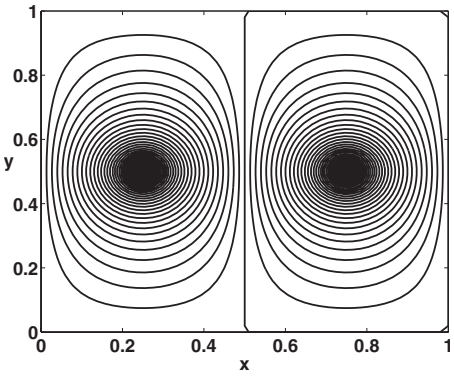

FIG. 2. Flow topology ψ associated with the steady point-vortex flow $\boldsymbol{u}_1$ according to (19).

For brevity, ψ and Ψ denote both the Hamiltonian and the corresponding topology hereafter. Important to note is that the present heat-transfer problem is restricted to solenoidal and inviscid flow of an incompressible fluid with constant material properties [37]. These constraints simplify the conservation law in the Lagrangian transport template (6) for fluid and thermal transport to $\boldsymbol{\nabla}\cdot\boldsymbol{u}=0$ and

$$\frac{\partial T}{\partial t}+\mu\boldsymbol{u}\cdot\boldsymbol{\nabla}T=\frac{\mu}{\mathrm{Pe}}\nabla^2 T, \tag{20}$$

respectively, which can be done without loss of generality [38,39].

The thermal transport corresponding with the point-vortex flows $\boldsymbol{u}_1$ and $\boldsymbol{u}_2$ is evaluated by numerical resolution of the advection-diffusion form (20) of the conservation law in (6) with thermal boundary conditions (17) and uniform initial temperature field $T(\boldsymbol{x},0)=1$. Numerical discretization of this initial-boundary-value problem employs a spectral method based upon Fourier-Chebyshev expansion of T in combination with a second-order Crank-Nicholson time-marching scheme and implementation of boundary conditions via the Lanczos tau method [40]. Integration of the kinematic equation in (6) is carried out with an explicit third-order Taylor-Galerkin scheme using velocity-field interpolation based upon the spectral expansion of $\boldsymbol{u}$. Isolation of the steady Hamiltonian from (9) follows from inversion of the spectral representation of the gradient operator.

B. Steady conditions

The flow domain has solid walls impermeable to fluid and thus the steady flow topology ψ comprises entirely of islands (Sec. III). Here ψ consists of two adjacent islands, each associated with one point vortex, as shown in Fig. 2. Physically, these islands entrap fluid indefinitely and set up clockwise (left-hand island) and counterclockwise (right-hand island) circulations via the concentric annuli. Such islands are the topological indicators of poor-mixing flows [4].

Steady thermal transport is in general not automatic with steady flow; this depends on the particular initial and boundary conditions for the associated initial-boundary-value problem. However, numerical analysis reveals that the present configuration admits a steady temperature field T for any Pe.

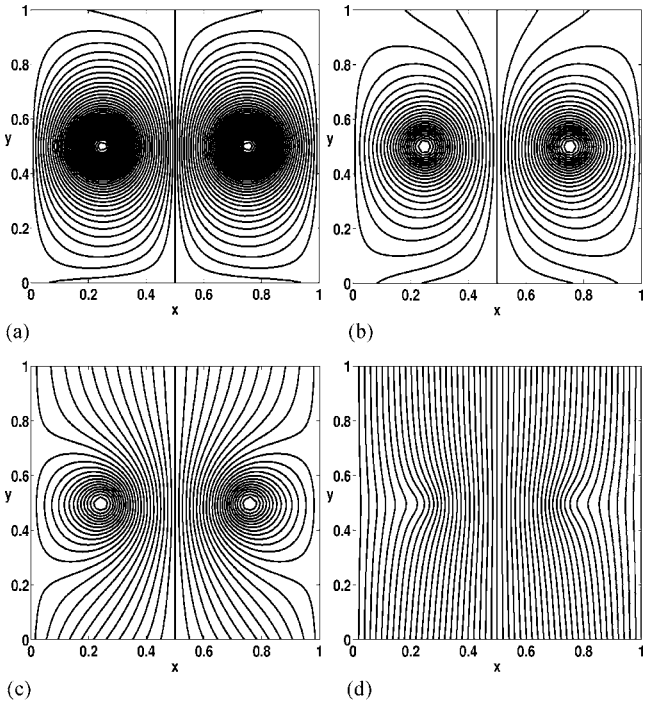

FIG. 3. Thermal topology Ψ associated with the steady flow $\boldsymbol{u}_1$ following (19) as a function of Pe: (a) $\Psi_{\mathrm{Pe}=100}$; (b) $\Psi_{\mathrm{Pe}=10}$; (c) $\Psi_{\mathrm{Pe}=1}$; (d) $\Psi_{\mathrm{Pe}=0.1}$. Panels (a)–(c) give typical Ψ comprising of thermal path (trajectories connecting bottom and top walls) and thermal islands (closed concentric trajectories); panel (d) gives typical Ψ comprising entirely of the thermal path. The progression (a)–(d) demonstrates the transition from the advection-dominated state [panel (a)] to the diffusion-dominated state [panel (d)] with diminishing Pe.

Thus, the concepts for steady systems (Sec. III) apply to the heat transfer as well.

The present domain has adiabatic sidewalls and nonadiabatic bottom and top walls. This implies that transport conduits between bottom and top walls must and islands may form in the thermal topology Ψ (Sec. III). The transport conduits ("heat conduits") form the "thermal path" via which wall-wall and wall-fluid (WW and WF) heat transfer occurs. Islands, if existent, demarcate regions that are thermally isolated from the environment ("thermal islands") and act as transport barriers to heat transfer. Thus thermal path and thermal islands play opposing roles in that the former and latter structures facilitate and obstruct, respectively, heat transfer between flow regions and nonadiabatic walls. Figure 3 gives Ψ at several Pe. Panels (a)–(c) clearly reveal the thermal path, connecting the nonadiabatic bottom and top walls, sandwiched in between two thermal islands. The wide sections of the thermal path that attach to the nonadiabatic walls coincide with the thermal boundary layers; the contraction occurs in the internal flow outside these boundary layers. Panel (d) shows a typical case with Ψ consisting entirely of the thermal path.

The thermal topology Ψ has two asymptotic states: infinite Pe and vanishing Pe. Infinite Pe signifies purely advective heat transfer and, consequently, flow and thermal topologies identify $\Psi_{\mathrm{Pe}\to\infty}=\psi$ (Fig. 2). (Thermal paths form for any finite Pe; $\Psi_{\mathrm{Pe}\to\infty}$ is devoid of thermal paths and, consequently, constitutes a singular state [20,22].) Vanishing Pe, on the other hand, signifies purely diffusive heat transfer and, irrespective of flow conditions, leads to the linear temperature distribution $T(y)=T_0+y\Delta T$ (here $T_0=2$ and $\Delta T=1/2-2=-3/2$) and an associated thermal topology Ψ that consists entirely of a thermal path made up of vertical parallel heat conduits. [This situation in fact corresponds with the steady-state temperature distribution within a solid; here the fluid, in thermal sense, behaves as a solid.] Figure 3 demonstrates the progression from the advection-dominated state [panel (a)] to the diffusion-dominated state [panel (d)] with decreasing Pe. This progression is characterized by diminution of the thermal islands in favor of the thermal path; the thermal islands vanish altogether below $\mathrm{Pe}\approx 0.15$.

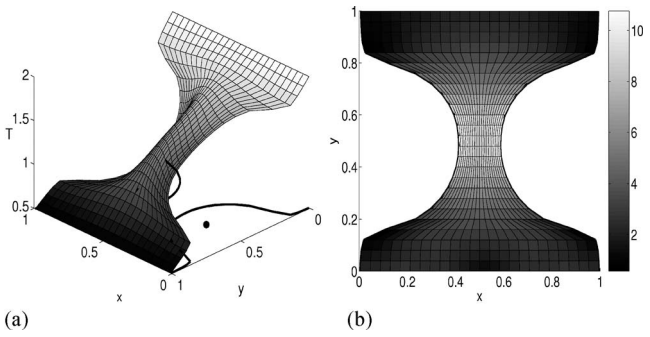

FIG. 4. Typical thermal path (Pe=2) and corresponding internal temperature distribution T [panel (a)] and total heat flux $\boldsymbol{v}T$ [panel (b)] for steady conditions. The curves in panel (a) outline the thermal path; the symbols indicate the point vortices.

The progression of the thermal topology with changing Pe (Fig. 3) is a direct consequence of the conservation law in (6). Figure 4 shows a typical thermal path (here for Pe=2) and its temperature distribution T [panel (a)] and total heat flux $\boldsymbol{v}T$ [panel (b)]. The gradual y-wise temperature decline signifies an approximately constant temperature gradient and, inherently, approximately constant diffusive heat flux throughout the thermal path. This attributes the dramatic increase in total heat flux through the thermal path [Fig. 4(b)] to advective heat transfer. By (6) this dictates convergence of heat-parcel trajectories and, given advection peaks at $y\approx 1/2$, progressive contraction of the thermal path in between the thermal boundary layers—and expansion of the thermal islands—with increasing Pe.

The thermal islands promote local thermal homogenization due to the thermal isolation from the environment. Figure 5 demonstrates this by the formation of "temperature plateaus" in the thermal islands that flatten with expansion of said islands for increasing Pe. The local thermal homogenization exposes the essentially heterogeneous temperature distribution in the thermal path; the thermal boundary layers (slopes at nonadiabatic walls) and the contraction (ridge connecting slopes) are clearly distinguishable. Expansion of the thermal islands progressively confines the thermal boundary layers, thus steepening the temperature gradient and augmenting the WW and WF heat transfer, and narrows the contraction, intensifying and concentrating the heat flux it carries. Thus, both homogeneity in the thermal islands and

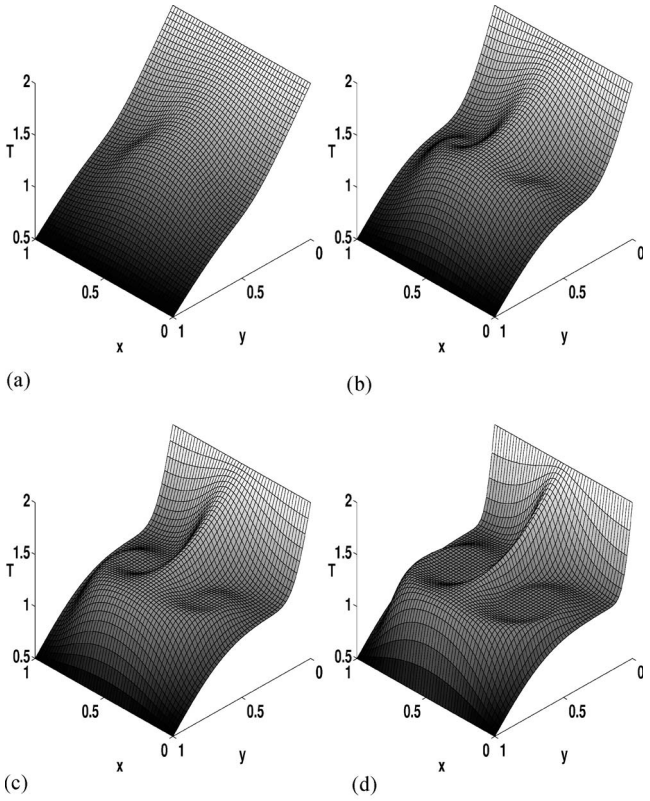

FIG. 5. Promotion of thermal homogenization by expansion of thermal islands for steady conditions: (a) Pe=2, (b) Pe=10, (c) Pe=30, (d) Pe=100. The progression demonstrates the formation of "temperature plateaus" due to expanding thermal islands for increasing Pe.

heterogeneity in the thermal path become more pronounced with growing Pe or, equivalently, with stronger advective heat transfer.

C. Time-periodic conditions

The time-periodic flow admits the decomposition $\boldsymbol{u}_2=\bar{\boldsymbol{u}}_2+\Delta\boldsymbol{u}_2$, with $\bar{\boldsymbol{u}}_2$ and $\Delta\boldsymbol{u}_2$ its steady and time-periodic components, respectively (Sec. III). The steady component identifies with the steady flow, i.e., $\bar{\boldsymbol{u}}_2=\boldsymbol{u}_1$, and, inherently, the baseline flow topology $\bar{\psi}$, associated with (16), coincides with the steady flow topology of $\boldsymbol{u}_1$ considered above.

The baseline flow topology $\bar{\psi}$ is subjected to time-periodic perturbation parametrized by μ. This results in progressive disintegration of the islands in $\bar{\psi}$ following well-known Hamiltonian scenarios with increasing perturbation parameter μ into a state of global chaos [35]. Figure 6 demonstrates this generic "route to chaos" for the present configuration. Panel (a) gives $\bar{\psi}$ in terms of its isopleths; panels (b)–(d) give ψ in terms of the Poincaré sections of an array of fluid parcels released on the line $y=1/2$. The progression clearly reveals the gradual diminution of both islands [panel (a)] in favor of a state of global chaos [panel (d)] with growing μ. Physically, this disintegration paves the way from

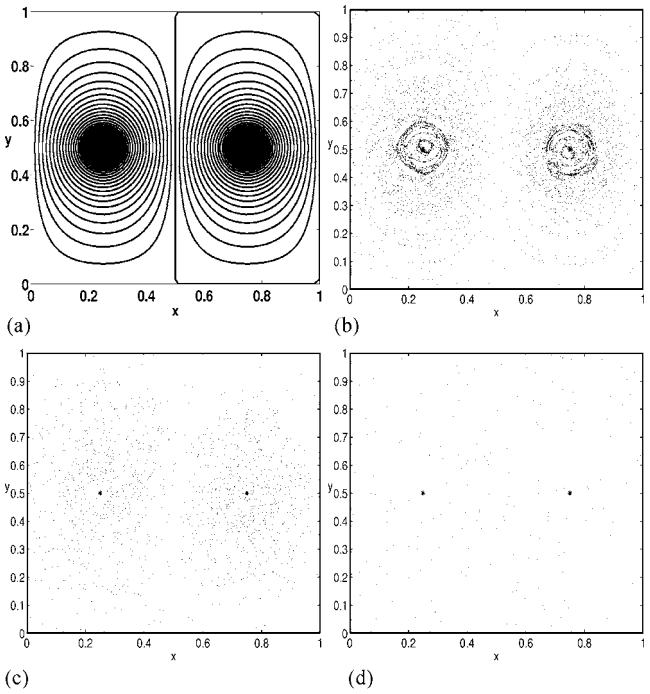

FIG. 6. Hamiltonian disintegration of the flow topology ψ from a regular state [panel (a)] into a globally chaotic state [panel (d)] with growing time-periodic perturbations (parametrized by μ): (a) $\mu=0$, (b) $\mu=0.03$, (c) $\mu=0.1$, (d) $\mu=1$. Shown are the Poincaré sections of an array of fluid parcels released on the line $y=1/2$.

poor-mixing ($\mu=0$) to good-mixing flows (μ beyond some threshold) [4].

The temperature field—and, inherently, its derived quantities—settles, irrespective of the flow conditions, in the moderate Pe range considered here for a time-periodic evolution with the same period time as the flow field. [Although, Fourier analysis reveals that the evolution is not of the form (19).] Figure 7 demonstrates this by means of the evolution of ΔT just beside the left vortex during two periods. Panel (a) gives the evolution for Pe=10 and shows that periodicity is maintained for advection ranging from weakly chaotic ($\mu=0.1$) to strongly chaotic ($\mu=5$); increasing μ intensifies the fluctuations and, for strongly chaotic conditions, introduces secondary oscillations. Panel (b) gives the evolution for $\mu=1$ (chaotic advection) and discloses similar behavior in Pe: Periodicity persists for a wide Pe range and fluctuations intensify and develop secondary oscillations with increasing Pe. Figure 8 demonstrates the regularity of the temperature field at $\mu=5$ and Pe=10 (chaotic advection) *in toto* for several time instances during one period.

The persistent periodicity in the present Pe regime reflects the regularizing effect of diffusion upon the thermal transport and is reminiscent of the coexistence of regular temperature distributions and chaotic advection observed in spatially periodic flows [13]. For purely advective conditions, temperature fluctuations become stochastic in regions with chaotic advection. Purely advective episodes—and thus said stochastic fluctuations—may in fact already occur in the high-Pe range [21,22]. This strongly suggests that above some (μ-dependent) Pe threshold the global time-periodic evolu-

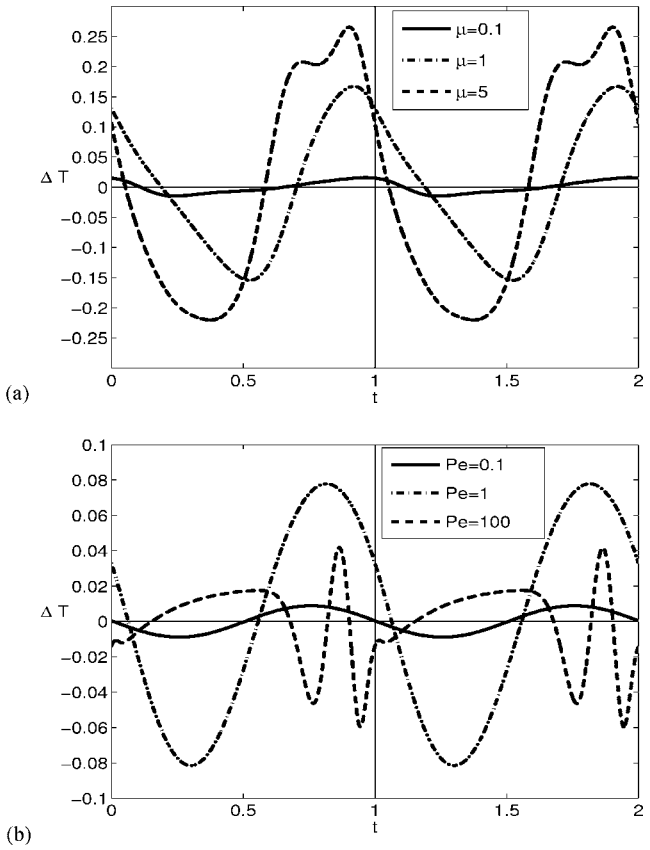

FIG. 7. Time periodicity of the temperature demonstrated by the evolution of ΔT just beside the left-hand vortex during two periods for various Pe and μ: (a) Pe=10, (b) $\mu=1$. The time periodicity is maintained for advection conditions ranging from weakly chaotic ($\mu=0.1$) to strongly chaotic ($\mu=5$).

tion breaks down (locally) in case of chaotic advection. The emergence of secondary oscillations for cases with significant chaotic advection, i.e., $(\mu,\mathrm{Pe})=(5,10)$ and $(\mu,\mathrm{Pe})=(1,100)$ in Fig. 7, in fact appear indicative of an imminent breakdown. Further pursuit of this issue may employ the concepts of inertial manifolds and strange eigenmodes known from mixing of diffusive tracers [11–13]. This is beyond the present scope, however.

The thermal islands in $\bar{\Psi}$ undergo changes essentially similar to that of their flow-topology counterparts upon time-periodic perturbation: Progressive disintegration into chaotic regions with increasing μ. Figure 9 demonstrates this breakdown for Pe=10. Panel (a) gives $\bar{\Psi}$ (isopleths); panels (b)–(d) give Ψ in terms of Poincaré sections. The progression clearly is qualitatively similar to that shown in Fig. 6 in that increasing μ effectuates gradual disintegration of both islands into chaotic regions.

The breakdown of the thermal islands introduces a fundamental change in transport properties that is specific for the thermal transport due to the presence of nonadiabatic walls. Heat-parcel trajectories, closed and entrapped within the islands for $\mu=0$, extend from the chaotic region and attach to the nonadiabatic walls. The Poincaré sections in Figs. 9(b)–9(d) correspond with one single heat parcel per thermal

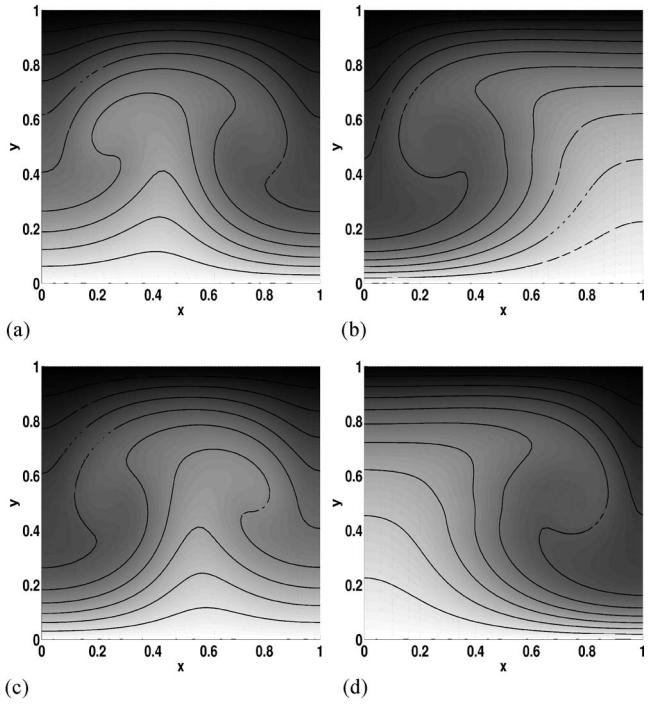

FIG. 8. Regularity of the temperature field demonstrated for $\mu=5$ and Pe=10 (chaotic advection) at several instances during one period: (a) $t=0$, (b) $t=1/4$, (c) $t=1/2$, (d) $t=3/4$.

island. Progression in time results in chaotic dispersion and, eventually, attachment to the cold top wall (upper string of symbols); regression in time, conversely, leads to attachment to the hot bottom (lower string of symbols). The dual attachment is a direct consequence of Reynolds' transport theorem [31] and implies that the heat-parcel trajectory has become part of a heat conduit. This behavior is typical for generic heat-parcel trajectories and has the important physical implication that the thermal islands disintegrate into chaotic heat conduits that, inherently, join the thermal path. Thus, the thermal isolation of the regions occupied by the thermal islands is lifted by the time-periodic perturbation.

The thermal path consists of heat conduits emanating from the hot bottom wall. This admits investigation of its response to time-periodic perturbation in terms of the Poincaré section of an equidistant grid of heat parcels released at the bottom wall at several time instances during one period. Figure 10(a) shows the thermal path at $\mu=0.1$; heavy and normal symbols indicate regular and chaotic heat conduits, respectively. [Heat conduits that cross the midplane $y=1/2$ only once are denoted regular, otherwise chaotic.] The shown Poincaré section is for Pe=10 representative for the situation at any $0\leq\mu\leq0.1$. This implies that the thermal path, notwithstanding extension by chaotic heat conduits due to disintegration of thermal islands, basically remains unaffected in the breakdown range $0\leq\mu\leq0.1$ of said islands. The regular heat conduits continue accounting for the WW and WF heat transfer. The chaotic heat conduits randomly attach at the nonadiabatic walls at isolated spots and yield a negligible contribution to said heat transfer. Thus, the chaotic seas, though connected with the nonadiabatic walls, by and large maintain the thermal isolation of the underlying thermal islands.

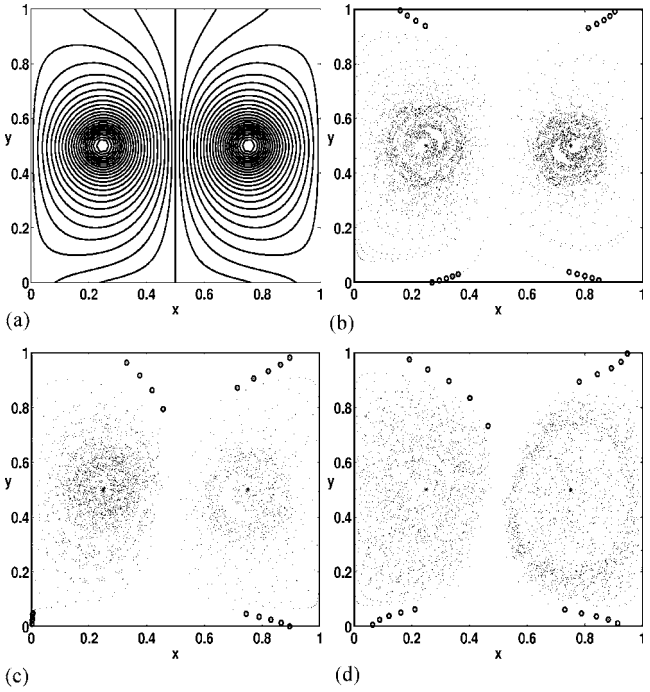

FIG. 9. Hamiltonian disintegration of the thermal islands of the baseline topology $\bar{\Psi}$ [panel (a)] into chaotic seas with growing time-periodic perturbations (parametrized by μ) for Pe=10: (a) $\mu=0$, (b) $\mu=0.05$, (c) $\mu=0.08$, (d) $\mu=0.1$. Panel (a) gives $\bar{\Psi}$ (isopleths); panels (b)–(d) give Ψ in terms of Poincaré sections of one single heat parcel per thermal island. Heat-parcel trajectories for $\mu>0$ typically attach to the nonadiabatic walls [lower and upper strings of symbols in panels (b)–(d) indicate last positions prior to attachment to bottom and top walls, respectively] and thus form chaotic heat conduits.

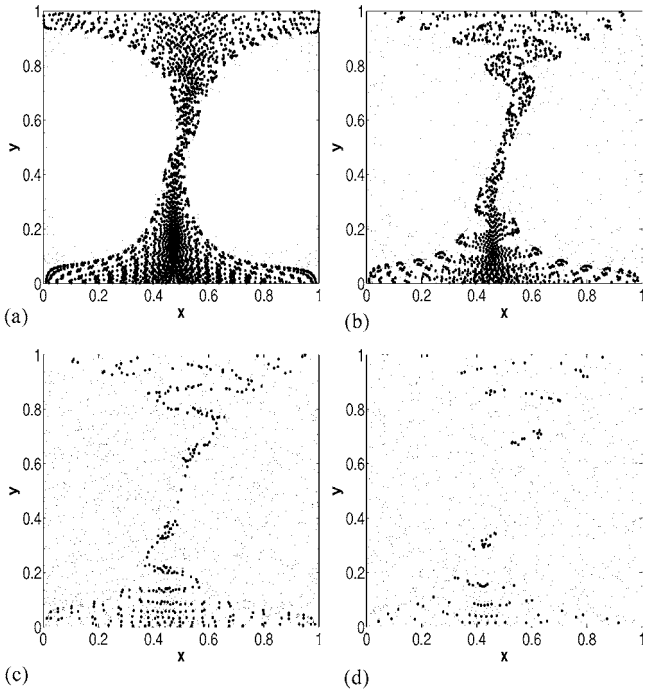

FIG. 10. Hamiltonian "chaotization" of the thermal path of the baseline topology $\bar{\Psi}$ with growing time-periodic perturbations (parametrized by μ) for Pe=10: (a) $\mu=0.1$, (b) $\mu=0.15$, (c) $\mu=0.2$, (d) $\mu=0.3$. Shown are the Poincaré sections of an equidistant grid of heat parcels released at the hot bottom wall at several time instances during one period; heavy and normal symbols indicate regular and chaotic heat conduits, respectively.

The regular heat conduits that make up the bulk of the thermal path in the range $0\leq\mu\leq0.1$ rapidly turn chaotic upon increasing μ beyond $\mu=0.1$ (Fig. 10). Thus, the thermal path physically changes from a regular arrangement of adjacent heat conduits contracting at the midplane $y=1/2$ to an intricate web of intertwined heat conduits covering the entire flow domain. This signifies transition from regular to chaotic heat transfer. The wall-wall heat transfer, consequently, transforms from directional to chaotic; the wall-fluid heat transfer transforms from localized to global. Thus the "chaotization" of the thermal path establishes "thermal communication" between the nonadiabatic walls and the entire flow domain.

The previous reveals that time-periodic perturbation induces a two-stage transition from regular to chaotic heat transfer with increasing μ. The first stage involves breakdown of the thermal islands into chaotic heat conduits while the original thermal path remains basically intact. The second stage involves "chaotization" of the thermal path into an intricate tangle of heat conduits covering the entire flow domain. For Pe, other than the case Pe=10 considered above, in essence the same happens yet within a different μ range; changes brought on by variation of Pe are in principle restricted to two quantitative effects. First, the thermal islands (Fig. 3) and, consequently, the ensuing chaotic seas of the first stage become more localized with decreasing Pe. Second, decreasing Pe delays the total transition by enlarging the μ ranges of the first and second stages yet without qualitatively affecting the progressions.

The delay in transition caused by decreasing Pe is demonstrated in Fig. 11 for the chaotic conditions at $\mu=1$ [Fig. 6(d)]. Panel (a) gives the Poincaré sections of both regular and chaotic heat-parcel trajectories originating from the hot bottom wall; panel (b) gives the regular trajectories for this state as projection into the physical domain $\mathcal{D}$. Decreasing Pe leads to a significant increase in regular trajectories (and thus heat conduits) under identical chaotic conditions [panels (b)–(d)]. The case Pe=0.1 is fully devoid of chaotic heat conduits and their nearly parallel arrangement, similar as the state shown in Fig. 3(d), mirrors the strongly diffusive nature of the heat transfer. [Decreasing Pe in a similar manner delays the emergence of secondary oscillations in the time-periodic evolution of the temperature field (Fig. 7).] This is another manifestation of the regularizing effect of diffusion upon the heat transfer.

The "chaotization" of the thermal transport promotes thermal homogenization in a manner reminiscent of that effectuated by chaotic advection in mixing flows [4]. The local thermal homogenization in the thermal islands is intensified by the disintegration into chaotic seas during the first stage of the transition from regular to chaotic heat transfer. Figures 12(a) and 12(b) show the time-averaged temperature field $\bar{T}$ under weakly chaotic conditions ($\mu=0.1$) for Pe=10 and

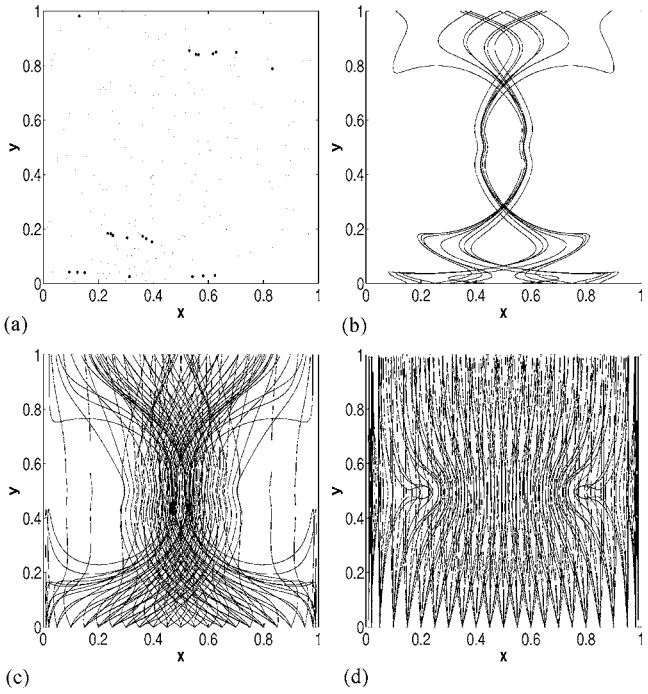

FIG. 11. Diffusion-induced delay of the "chaotization" (and inherent regularization) of the thermal path under chaotic-advection conditions ($\mu=1$). Panel (a) gives the Poincaré sections of both regular and chaotic heat-parcel trajectories originating from the hot bottom wall at Pe=10; panel (b) gives the corresponding projection of the regular trajectories into the physical domain $\mathcal{D}$; panels (c) and (d) give these projections for Pe=1 and Pe=0.1.

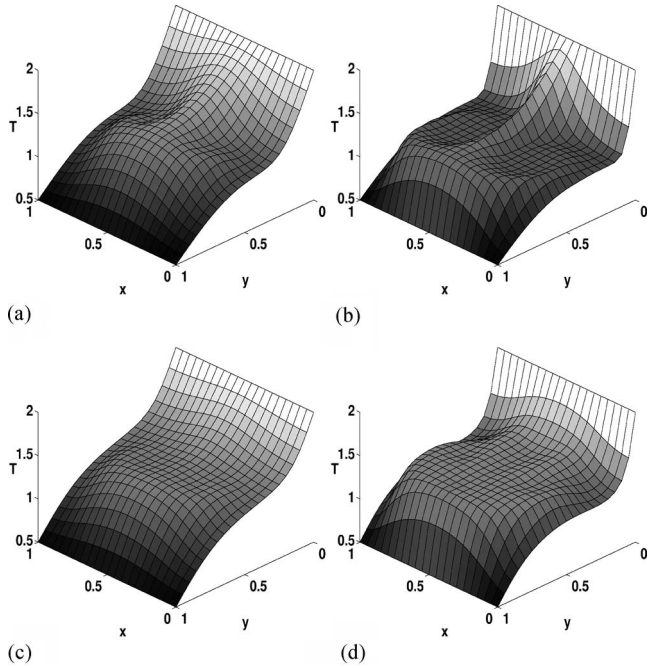

FIG. 12. Promotion of thermal homogenization by "chaotization" of thermal transport demonstrated by the time-averaged temperature field $\bar{T}$: (a) $\mu=0.1$, Pe=10; (b) $\mu=0.1$, Pe=100; (c) $\mu=5$, Pe=10; (d) $\mu=1$, Pe=100. First stage (weakly chaotic conditions), expansion of temperature plateaus due to disintegration of thermal islands into chaotic seas [panels (a) and (b)]; second stage (strongly chaotic conditions), thermal homogenization throughout the interior of the domain due to "chaotization" of the thermal path [panels (c) and (d)].

Pe=100, respectively, and reveals an expansion of the temperature plateaus relative to the corresponding steady situation (Fig. 5). However, changes are marginal and predominantly restricted to the interior; the thermal boundary layers are virtually unaffected. The second stage of the transition is characterized by "chaotization" of the thermal path due to strongly chaotic conditions. This destroys the separation between the chaotic seas and, consequently, gives rise to thermal homogenization throughout the interior of the flow domain. Figures 12(c) and 12(d) demonstrate this for the first-stage situations in Figs. 12(a) and 12(b), respectively. The ridge in the temperature fields, coinciding with the contraction of the regular thermal path, has vanished in favor of a substantially homogenized state in between the thermal boundary layers.

D. Heat exchange with the environment

The above demonstrated the significant effect of time-periodic perturbations upon the thermal topology and, consequently, the thermal transport within the flow domain. Intimately related to this is the effect of changing thermal topology upon the heat exchange between the nonadiabatic walls and the environment—and, inherently, the amount of heat transferred through the thermal path. To this end we introduce the Nusselt number [17]

$$\mathrm{Nu} = \frac{Q}{Q_d} = \frac{1}{\Delta T}\int_0^1 \int_0^1 \frac{\partial T}{\partial y}(x,0,t)\,dx\,dt, \tag{21}$$

which gives the ratio of the actual (Q) to diffusion-only (Q_d) heat flux (i.e., $\mathrm{Nu}_{\mathrm{Pe}=0}=1$ for all μ) across the bottom wall, with $\Delta T<0$ as the imposed temperature drop between the nonadiabatic walls. [Nu according to (21) may be employed for both steady and time-periodic conditions.] Figure 13 gives Nu as a function of Pe for the steady flow and the time-periodic flow under weakly chaotic ($\mu=0.1$) and strongly chaotic ($\mu=1$) conditions. The Nusselt number Nu switches smoothly from the diffusion-only limit (Nu=1; horizontal asymptote) to the advective-diffusive state ($\mathrm{Nu}\sim\sqrt{\mathrm{Pe}}$; skew asymptote) with increasing Pe [41,44].

The substantial increase in Nu with growing Pe (Fig. 13) is consistent with other studies [13,17,18] and exposes the instrumental role of advection in heat-transfer enhancement. However, the kind of advection (i.e., steady vs time periodic; regular vs chaotic) appears practically immaterial for the heat flux across the boundary; shown profiles virtually coincide. This is a direct consequence of the thermal heterogeneity imposed upon the system by maintaining bottom and top walls at different temperatures. Thus, thermal boundary layers of thickness $\delta\sim\mathrm{Pe}^{-1/2}$ form at these walls within which heat transfer occurs primarily by diffusion; advection, of whatever kind, is of secondary importance only in such

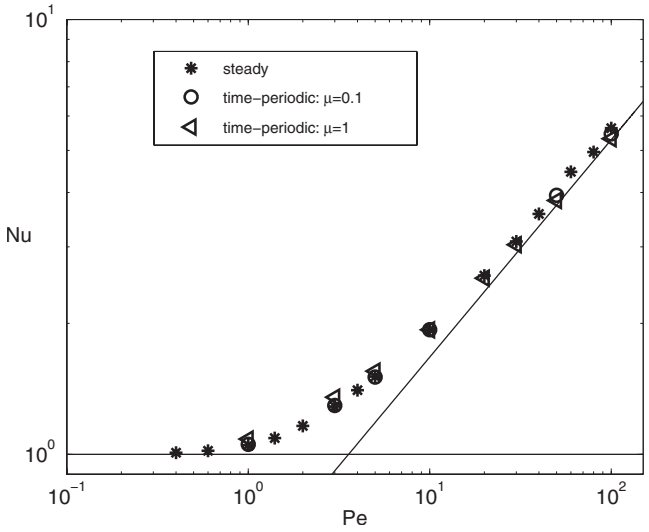

FIG. 13. Heat exchange between nonadiabatic walls and environment in terms of the Nusselt number Nu according to (21). Nu is given as a function of Pe for the steady flow and the time-periodic flow under weakly chaotic ($\mu=0.1$) and strongly chaotic ($\mu=1$) conditions. The horizontal asymptote corresponds with the diffusion-only limit Nu=1; the skew asymptote corresponds with the advective-diffusive state $\mathrm{Nu}\sim\sqrt{\mathrm{Pe}}$.

boundary layers [42,44]. This is evident from the temperature fields for steady (Fig. 5) and time-periodic (Fig. 12) conditions. The spatial extent (and corresponding local thermal topology) of the thermal boundary layers—and, consequently, the heat flux across the walls—is, regardless of the flow conditions, predominantly dependent upon Pe. The interior temperature distribution in between said boundary layers is, as found before, inextricably linked with the flow conditions, on the other hand.

The above reveals that, despite popular notions, transport enhancement is not necessarily synonymous to chaotic advection; this depends heavily on the type of transport problem. Chaotic advection is a well-established mechanism for accomplishment of the (thermal) homogenization relevant for mixing [4] and reactive [19] processes and, intimately related to homogenization, efficient transport under heat-flux boundary conditions [13,18]. For fundamentally heterogeneous transport problems as that considered here (i.e., WW and WF heat transfer in the case of nonadiabatic walls maintained at different temperatures), the role of advection—and then in particular its interplay with diffusion—proves much more subtle. Studies on similar configurations support this [16,13].

V. CONCLUSIONS

The present study proposes a unified Lagrangian transport template for topological description of advective (fluid) and advective-diffusive (scalar) transport under laminar flow conditions. This unified description rests on the expression of scalar transport as purely advective transport by the total scalar flux. The underlying rationale is that scalar flux fundamentally is the transport of "scalar parcels" by the total scalar flux in an analogous manner as fluid motion is the transport of fluid parcels by the flow. This unified approach admits generalization of the concept of transport topologies known from laminar mixing studies to scalar transport. The study is restricted to two-dimensional systems and, due to the continuity constraint in the unified Lagrangian transport template, the transport topologies of fluid as well as scalar transport are Hamiltonian.

The Hamiltonian structure of the unified Lagrangian model dictates that steady transport topologies comprise two elementary building blocks, islands and transport conduits. The former entrap and isolate material and act as transport barriers; the latter facilitate exchange of material with and between permeable walls. Time periodicity causes Hamiltonian disintegration of the steady transport topologies. This generically leads to intricate transport topologies and chaotic transport. Transport conduits are invariably present in the transport topology of any (un)steady system with permeable walls and form the fundamental topological entities by which scalar exchange between permeable walls and flow occur. Moreover, transport conduits signify essentially heterogeneous transport conditions.

The unified Lagrangian transport template is demonstrated for the heat transfer in a steady and time-periodic point-vortex flow within a bounded square domain with adiabatic sidewalls and nonadiabatic bottom and top walls. The steady flow topology consists, due to the solid boundary, entirely of islands. The thermal topology invariably comprises transport conduits that form between the nonadiabatic walls ("thermal path") and, depending on system parameters, may comprise "thermal islands" that constitute regions thermally isolated from the environment. The thermal path facilitates wall-wall and wall-fluid (WW and WF) heat transfer; the thermal islands form thermally isolated regions within which thermal homogenization occurs.

Time periodicity causes Hamiltonian disintegration of the islands of the steady flow topology into a global chaotic sea. The thermal topology undergoes a similar transition from a regular to a chaotic state, albeit in two stages; the first and second stages correspond with "weak" and "strong" time-periodic perturbations. The first stage involves disintegration of the thermal islands into chaotic heat conduits while the thermal path basically remains intact. However, though this strictly lifts the thermal isolation of the occupied regions, the heat exchange with the nonadiabatic walls is negligible. The second stage causes the thermal path to become chaotic and expand throughout the entire flow domain. This "chaotization" of the thermal path establishes "thermal communication" between the nonadiabatic walls and the entire flow domain and promotes thermal homogenization outside the thermal boundary layers. Increasing diffusion delays the transition and permits for the coexistence of chaotic advection with (locally) regular heat transfer.

The role of advection in heat-transfer enhancement is subtle. Advection in itself substantially increases the heat exchange with—and, inherently, between—the nonadiabatic walls and, consequently, the overall WW and WF heat transfer. The kind of advection proves virtually immaterial in this respect, though; heat flux across the boundary appears for any flow conditions dependent primarily on Pe. This is due

to the prevailing role of diffusive transport in the thermal boundary layers that basically overrules any form of advective transport. The state in between the thermal boundary layers, on the other hand, depends significantly on the kind of advection. Thermal homogenization in the interior of the flow domain increases with growing degree of disorder in a manner akin to that known from chaotic mixing.

The Lagrangian transport template admits generalization to any transport problem governed by a conservation law of the form (6) and flux field $\boldsymbol{v}$ of arbitrary composition. Any such 2D (un)steady and 3D steady transport problem in principle has a Hamiltonian structure and corresponding transport topology that is essentially similar to that demonstrated here. This holds independently of specific fluid rheology or thermodynamical behavior and coupling between scalar and fluid transport (e.g., temperature-dependent fluid properties) and thus means that the proposed Lagrangian approach is applicable to a wide range of flow configurations. The present approach furthermore admits extension to higher-order systems. 3D unsteady systems with solenoidal flux vectors $\boldsymbol{v}$, i.e., $\boldsymbol{\nabla}\cdot\boldsymbol{v}=0$, permit a unified Lagrangian-topological approach based upon Liouvillian maps [43]. 3D unsteady systems with nonsolenoidal $\boldsymbol{v}$ can be reconciliated with the concept of Liouvillian maps [34] by recasting the associated 3D conservation law, similar to the course of action underlying (11), in terms of a four-dimensional time-space domain. Studies to address and demonstrate these issues are underway.

The unified Lagrangian transport template is believed to have great potential for practical application and then in particular to heterogeneous problems involving scalar exchange with permeable walls (e.g., heat transfer, mass exchange with porous walls). The proposed approach namely admits systematic visualization and investigation of the fluid-structure interactions that facilitate the, for many practical applications highly relevant, scalar exchange between fluids and walls. Diffusive transport—and thus the transport routes—furthermore continues through permeable walls, meaning that a global transport topology, i.e., encompassing both flow and permeable walls, can be identified in such configurations. Moreover, the unified Lagrangian transport template may be applied to analysis of systems involving multiple scalars. Isolation of the associated transport topologies for instance enables identification of the various distribution routes, isolated regions, and interaction zones.

ACKNOWLEDGMENT

The author is indebted to Dr. Guy Metcalfe (CSIRO Applied Fluid Chaos, Melbourne, Australia) for close reading of this paper.

APPENDIX: EXPRESSIONS FOR THE POINT-VORTEX FLOW

The 2D velocity field induced by a point vortex with strength γ located in the dimensional square domain $\bar{\mathcal{D}}=[0,L]\times[0,L]$ is, in complex notation, given by

$$u = u_x - iu_y = \frac{\gamma}{2\pi}[\zeta(z-z_1)+\zeta(z-z_2)-\zeta(z-z_3)-\zeta(z-z_4)], \tag{A1}$$

with $z_1=x_1+iy_1\in\bar{\mathcal{D}}$ the (complex) position of the point vortex, $z_{2,3,4}$ the positions of the corresponding shadow vortices, which indirectly implement the square boundary, as

$$z_2=(2L-x_1)+i(2L-y_1), \quad z_3=x_1+i(2L-y_1),$$

$$z_4=(2L-x_1)+iy_1, \tag{A2}$$

and ζ Weierstrass ζ functions [45]. The latter are, in terms of Laurent's series, defined as

$$\zeta(z)=z^{-1}H(z), \quad H(z)=1-\sum_{k=2}^{\infty}\frac{c_k}{(2k-1)}\left(\frac{z}{L}\right)^{2k}, \tag{A3}$$

with c_k expansion coefficients [45]. The complex velocity field (A1) may, using relation (A3), be rewritten as

$$u=\frac{\gamma}{2\pi}\left[\frac{(Hz-z_1)}{z-z_1}+\frac{H(z-z_2)}{z-z_2}-\frac{H(z-z_3)}{z-z_3}-\frac{H(z-z_4)}{z-z_4}\right], \tag{A4}$$

upon appreciating that $H(z)$ by definition is nondimensional leading to

$$u=\frac{\gamma}{2\pi L}\left(\frac{H(z'-z_1')}{z'-z_1'}+\frac{H(z'-z_2')}{z'-z_2'}-\frac{H(z'-z_3')}{z'-z_3'}-\frac{H(z'-z_4')}{z'-z_4'}\right)$$

$$=Uu', \tag{A5}$$

with $z'=z/L$ the nondimensional complex coordinate. This yields $U=\gamma/2\pi L$ as velocity scale for the nondimensional parameters (7) and

$$u'=\frac{H(z'-z_1')}{z'-z_1'}+\frac{H(z'-z_2')}{z'-z_2'}-\frac{H(z'-z_3')}{z'-z_3'}-\frac{H(z'-z_4')}{z'-z_4'}, \tag{A6}$$

as nondimensional velocity in the unit square $\mathcal{D}=[0,1]\times[0,1]$. The basic velocities $\boldsymbol{u}_+$ and $\boldsymbol{u}_-$ in the steady and time-periodic flow fields (19) coincide with (A6) for $z_1=1/4+i/2$ and $z_1=3/4+i/2$, respectively, and $z_{2,3,4}$ according to (A2).

[1] S. P. Beerens, H. Ridderinkhof, and J. T. F. Zimmerman, Chaos, Solitons Fractals **4**, 1011 (1994).
[2] S. Wiggins, Annu. Rev. Fluid Mech. **37**, 295 (2005).
[3] J. Korenaga and P. B. Kelemen, Earth Planet. Sci. Lett. **156**, 1 (1998).
[4] H. Aref, Phys. Fluids **14**, 1315 (2002).
[5] J. M. Ottino and S. Wiggins, Philos. Trans. R. Soc. London, Ser. A **362**, 923 (2004).
[6] H. A. Stone, A. D. Stroock, and A. Ajdari, Annu. Rev. Fluid Mech. **36**, 381 (2004).
[7] H. A. Stone and S. Kim, AIChE J. **47**, 1250 (2001).
[8] S. Cerbelli, V. Vitacolonna, A. Adrover, and M. Giona, Chem. Eng. Sci. **59**, 2125 (2004).
[9] M. Giona, S. Cerbelli, and V. Vitacolonna, J. Fluid Mech. **513**, 221 (2004).
[10] M. Giona, V. Vitacolonna, S. Cerbelli, and A. Adrover, Phys. Rev. E **70**, 046224 (2004).
[11] W. Liu and G. Haller, Physica D **188**, 1 (2004).
[12] W. Liu and G. Haller, Physica D **194**, 297 (2004).
[13] D. R. Lester, M. Rudman, G. Metcalfe, and H. Blackburn, J. Comput. Phys., **227**, 3032 (2008).
[14] M. Giona, S. Cerbelli, and A. Adrover, Phys. Rev. Lett. **88**, 024501 (2001).
[15] M. Abel, A. Celani, D. Vergni, and A. Vulpiani, Phys. Rev. E **64**, 046307 (2001).
[16] H.-C. Chang and M. Sen, Chaos, Solitons Fractals **4**, 955 (1994).
[17] D. R. Sawyers, M. Sen, and H.-C. Chang, Int. J. Heat Mass Transfer **41**, 3559 (1998).
[18] T. Lemenand and H. Peerhossaini, Appl. Therm. Eng. **22**, 1717 (2002).
[19] I. Z. Kiss, J. H. Merkin, and Z. Neufeld, Phys. Rev. E **70**, 026216 (2004).
[20] S. W. Jones, Chaos, Solitons Fractals **4**, 929 (1994).
[21] X. Z. Tang and A. H. Boozer, Physica D **95**, 283 (1996).
[22] X. Z. Tang and A. H. Boozer, Phys. Fluids **11**, 1418 (1999).
[23] E. Shuckburgh and P. Haynes, Phys. Fluids **15**, 3342 (2003).
[24] S. Wiggins and J. M. Ottino, Philos. Trans. R. Soc. London, Ser. A **362**, 937 (2004).
[25] M. Speetjens, G. Metcalfe, and M. Rudman, Phys. Fluids **18**, 103103 (2006).
[26] G. K. Batchelor, *An Introduction to Fluid Dynamics* (Cambridge University Press, Cambridge, 1967).
[27] This concept holds for generic $\boldsymbol{u}$. Hence, fluid rheology and coupling between fluid properties and the scalar, etc., are immaterial in the present context.
[28] Redefinition simply involves linear shifting of the original definition ϕ' to $\phi=\phi'+\phi_0$, with ϕ_0 an arbitrary constant such that $\phi>0$, and (if present) reformulation of nonhomogeneous Dirichlet conditions on the boundary. Addition of the constant ϕ_0 has no effect upon the dynamics, as the diffusive transport is determined entirely by gradients of ϕ.
[29] The Péclet number strictly concerns heat transfer. For brevity, it here refers to generic scalar transport.
[30] The limit $\mathrm{Pe}\to\infty$, corresponding with the purely advective fluid transport, in fact is a singular limit [20,22] of the unified description (6). (Mathematically, unbounded Pe changes the type of the underlying PDE; physically, unbounded Pe renders the system reversible in time [22].) Hence, only finite Pe for scalar transport.
[31] P. K. Kundu, *Fluid Mechanics* (Academic, London, 1990).
[32] K. Bajer, Chaos, Solitons Fractals **4**, 895 (1994).
[33] Note that $\partial\dot{\boldsymbol{x}}/\partial t$ is not to be confused with the parcel acceleration $\ddot{\boldsymbol{x}}$.
[34] V. I. Arnol'd, *Mathematical Methods of Classical Mechanics* (Springer, New York, 1978).
[35] E. Ott, *Chaos in Dynamical Systems* (Cambridge University Press, Cambridge, 2002).
[36] V. V. Meleshko, Phys. Fluids **6**, 6 (1994).
[37] Solenoidality is a flow property and incompressibility is a fluid property and are not necessarily equivalent. Solenoidality via continuity yields $\frac{D\rho}{Dt}=0$ and thus renders ρ a conserved quantity. For uniform initial density distributions this implies constant ρ at any time. Incompressibility means that $\rho=\rho(p,T)$ is independent of the pressure p and, inherently, is temperature dependent only, $\rho=\rho(T)$. For isothermal systems $\rho=\rho(T)$ implies constant ρ and, consequently, solenoidality and incompressibility are equivalent under these conditions. However, for nonisothermal systems $\rho=\rho(T)$ via continuity implies $\nabla\cdot\boldsymbol{u}=-\frac{1}{\rho}\frac{D\rho}{Dt}=-\frac{1}{\rho}\frac{d\rho}{dT}\frac{DT}{Dt}$ and, consequently, solenoidality and incompressibility are equivalent only if at least one of the following conditions is fulfilled: (i) $\frac{DT}{Dt}=0$; (ii) $\frac{d\rho}{dT}=0$. The former implies absence of diffusive heat transfer and thus is invalid within the present scope. Hence, accommodating both solenoidality and incompressibility here requires $\frac{d\rho}{dT}=0$ and, via $\rho=\rho(T)$, constant ρ.
[38] The point-vortex flow, though inviscid and solenoidal, is representative of generic laminar flows with variable density. The two fundamental properties underlying the unified Lagrangian transport template (6) are namely upheld by the point-vortex flow. First, the point-vortex flow, such as laminar flows, is deterministic; fluid rheology is immaterial in the present context. Second, the point-vortex flow satisfies continuity and thus, as generic 2D flows satisfying continuity, implies Hamiltonian flow topologies.
[39] Generic advective-diffusive energy transfer is (in dimensional form and omitting viscous dissipation and kinetic and potential contributions) governed by (i) $\partial(\rho e)/\partial t+\nabla\cdot(\rho h\boldsymbol{u}-\lambda\nabla T)=0$, with e and h the internal energy and enthalpy, respectively, and λ the thermal conductivity [26]. The conservation law (i) assumes a form essentially identical to (6) via (ii) $\partial(\rho e)/\partial t+\nabla\cdot(\rho e\boldsymbol{v})=0$, $\boldsymbol{v}=(h/e)\boldsymbol{u}-(\lambda/\rho e)\nabla T$, upon implementation of solenoidality ($\nabla\cdot\boldsymbol{u}=0$), incompressibility ($e=h=c_pT$ and, for $\nabla\cdot\boldsymbol{u}=0$, constant ρ) and constant λ, c_p leading to the dimensional form of the advection-diffusion equation (20). The latter constitutes a strong simplification of (ii) yet retains its fundamental structure and properties and, consequently, is qualitative representative for generic heat-transfer problems governed by (ii).
[40] C. Canuto, M. Y. Hussaini, A. Quarteroni, and T. A. Zang, *Spectral Methods in Fluid Dynamics* (Springer, Berlin, 1987).
[41] The advective-diffusive state leads to the formation of thermal boundary layers on the nonadiabatic walls. For isothermal walls this implies $\mathrm{Nu}=f(\mathrm{Pr})\sqrt{\mathrm{Re}}$, with $\mathrm{Re}=UL/\nu$ and $\mathrm{Pr}=\nu/\alpha$ the well-known Reynolds and Prandlt numbers, respectively, and ν the kinematic viscosity of the fluid [44]. Through $\mathrm{Re}=\mathrm{Pe}/\mathrm{Pr}$ this gives $\mathrm{Nu}=g(\mathrm{Pr})\sqrt{\mathrm{Pe}}$, with $g(\cdots)$ some functional in Pr that, since Pr may be chosen arbitrarily due to the fact that the point-vortex flow is inviscid, yields $\mathrm{Nu}\sim\sqrt{\mathrm{Pe}}$.
[42] Thermal boundary layers are, for the present case of flow fields

decoupled from the thermal field, analogous to flow boundary layers [44]. This analogy admits translation of the typical boundary-layer thickness $\delta \sim \mathrm{Re}^{-1/2}$ for flows [31] to $\delta \sim \mathrm{Pe}^{-1/2}$ as typical boundary-layer thickness for the thermal field.

[43] J. H. E. Cartwright, M. Feingold, and O. Piro, Physica D **76**, 22 (1994).

[44] H. Schlichting and K. Gersten, *Boundary-Layer Theory* (Springer, Berlin, 2000).

[45] M. Abramowitz and I. A. Stegun, *Handbook of Mathematical Functions* (Dover, New York, 1972).